

ARTICLE

Received 21 Jan 2015 | Accepted 9 Nov 2015 | Published 7 Jan 2016

DOI: 10.1038/ncomms10147

OPEN

Local admixture of amplified and diversified secreted pathogenesis determinants shapes mosaic *Toxoplasma gondii* genomes

Hernan Lorenzi^{1,*}, Asis Khan^{2,3,*}, Michael S. Behnke^{2,4,*}, Sivaranjani Namasivayam^{5,6}, Lakshmi Puram S. Swapna^{7,8}, Michalis Hadjithomas^{1,†}, Svetlana Karamycheva¹, Deborah Pinney⁹, Brian P. Brunk⁹, James W. Ajioka¹⁰, Daniel Ajzenberg¹¹, John C. Boothroyd¹², Jon P. Boyle¹³, Marie L. Dardé¹¹, Maria A. Diaz-Miranda⁹, Jitender P. Dubey¹⁴, Heather M. Fritz¹⁵, Solange M. Gennari¹⁶, Brian D. Gregory⁹, Kami Kim¹⁷, Jeroen P.J. Saeij¹⁸, Chunlei Su¹⁹, Michael W. White²⁰, Xing-Quan Zhu²¹, Daniel K. Howe²², Benjamin M. Rosenthal¹⁴, Michael E. Grigg³, John Parkinson^{7,8}, Liang Liu^{23,24}, Jessica C. Kissinger^{5,6,24}, David S. Roos⁹ & L. David Sibley²

Toxoplasma gondii is among the most prevalent parasites worldwide, infecting many wild and domestic animals and causing zoonotic infections in humans. *T. gondii* differs substantially in its broad distribution from closely related parasites that typically have narrow, specialized host ranges. To elucidate the genetic basis for these differences, we compared the genomes of 62 globally distributed *T. gondii* isolates to several closely related coccidian parasites. Our findings reveal that tandem amplification and diversification of secretory pathogenesis determinants is the primary feature that distinguishes the closely related genomes of these biologically diverse parasites. We further show that the unusual population structure of *T. gondii* is characterized by clade-specific inheritance of large conserved haploblocks that are significantly enriched in tandemly clustered secretory pathogenesis determinants. The shared inheritance of these conserved haploblocks, which show a different ancestry than the genome as a whole, may thus influence transmission, host range and pathogenicity.

¹Department of Infectious Diseases, The J. Craig Venter Institute, 9704 Medical Center Drive, Rockville, Maryland 20850, USA. ²Department of Molecular Microbiology, Washington University School of Medicine, 660 S. Euclid Avenue, St Louis, Missouri 63130, USA. ³Laboratory of Parasitic Diseases, NIAID, National Institutes of Health, Bethesda, Maryland 20892, USA. ⁴Pathobiological Sciences, School of Veterinary Medicine, Louisiana State University, Baton Rouge Louisiana 70803, USA. ⁵Department of Genetics, University of Georgia, Athens, Georgia 30602, USA. ⁶Center for Tropical and Emerging Global Diseases, University of Georgia, Athens Georgia 30602, USA. ⁷Program in Molecular Structure and Function, Hospital for Sick Children, Toronto, Ontario, Canada M5G 1L7. ⁸Departments of Biochemistry and Molecular Genetics, University of Toronto, Toronto, Ontario, Canada M5S 1A8. ⁹Department of Biology, University of Pennsylvania, Philadelphia, Pennsylvania 19104, USA. ¹⁰Department of Pathology, University of Cambridge, Cambridge CB2 1QP, UK. ¹¹Biological Resource Center for Toxoplasma, INSERM, University Limoges, CHU Limoges, UMR_S 1094, Tropical Neuroepidemiology, Institute of Neuroepidemiology and Tropical Neurology, Limoges 87025, France. ¹²Department of Microbiology and Immunology, Stanford School of Medicine, Stanford, California 94305, USA. ¹³Department of Biological Sciences, Dietrich School of Arts and Sciences, University of Pittsburgh, Pittsburgh, Pennsylvania 15260, USA. ¹⁴Animal Parasitic Diseases Laboratory, Beltsville Agricultural Research Center, Agricultural Research Service, USDA, Beltsville, Maryland 20705, USA. ¹⁵Department of Veterinary Pathology and Microbiology, Washington State University, College of Veterinary Medicine, Pullman, Washington 99164, USA. ¹⁶Department of Preventive Veterinary Medicine and Animal Health, Faculty of Veterinary Medicine, University of São Paulo, São Paulo, SP CEP 05598-270, Brazil. ¹⁷Departments of Medicine, Pathology, and Microbiology and Immunology, Albert Einstein College of Medicine, Bronx, New York 10461, USA. ¹⁸Department of Pathology, Microbiology & Immunology, University of California, David, California 95616, USA. ¹⁹Department of Microbiology, University of Tennessee, Knoxville, Tennessee 37996, USA. ²⁰Departments of Molecular Medicine and Global Health, Florida Center for Drug Discovery and Development (CDDI), University of South Florida, 3720 Spectrum Boulevard, Suite 304, Tampa, Florida 33612, USA. ²¹State Key Laboratory of Veterinary Etiological Biology, Key Laboratory of Veterinary Parasitology of Gansu Province, Lanzhou Veterinary Research Institute, Chinese Academy of Agricultural Sciences, Lanzhou, Gansu Province 730046, China. ²²Department of Veterinary Science, University of Kentucky, Lexington, Kentucky 40546, USA. ²³Department of Statistics, University of Georgia, Athens Georgia 30602, USA. ²⁴Institute of Bioinformatics, University of Georgia, Athens, Georgia 30602, USA. * These authors contributed equally to this work. † Present address: Prokaryotic Super Program, DOE Joint Genome Institute, Walnut Creek, California 94598, USA. Correspondence and requests for materials should be addressed to H.L. (email: hlorenzi@jcvl.org) or to L.D.S. (email: sibley@wustl.edu).

Most of the diversity of eukaryotic life is contained in early branching, unicellular organisms that differ substantially from model organisms such as yeast, flies, worms and mice¹. This diversity is illustrated by the protozoan phylum Apicomplexa, estimated to contain more than 5,000 species², most being parasitic on insects and mollusks, while a few cause disease in domestic animals and/or humans³. Studies of these few disease-causing agents comprise our limited knowledge of this phylum, which demarcate a deep branching phylogeny that has been estimated to span more than ~400 my of evolution⁴ (Fig. 1a). Over that time frame, it is likely that apicomplexans have adapted to their various vertebrate hosts via multiple independent changes in host range, and yet the molecular mechanisms underlying these adaptations remain largely undefined.

Although most members of this phylum are adapted to a narrow range of hosts, *Toxoplasma gondii* stands out as a generalist. The genus is characterized by a single species that enjoys worldwide prevalence in animals including humans⁵. Infections with *T. gondii* are common⁶, yet they typically only cause disease in immunocompromised hosts, or as a result of transplacental infection⁷. *T. gondii* is equipped with excellent forward and reverse genetic tools, providing a model for many less-tractable apicomplexan parasites⁸. As a highly successful parasite, *T. gondii* is positioned to inform us about genomic features that are important for efficient transmission and expansion of host range. Here, we sought to exploit this potential by analysing the composition and diversity of the *T. gondii* genome in comparison to several closely related apicomplexan parasites.

T. gondii belongs to the tissue-cyst forming coccidian parasites, which is distinguished from enteric coccidian parasites by having an alternating two-host (heteroxenous) life cycle (Fig. 1a, Table 1)⁵. Most tissue-cyst forming coccidian parasites have obligatory heteroxenous life cycles (that is, *Sarcocystis* spp. and *Hammondia* spp.), while others share this mode but have evolved additional strategies for transmission (Table 1)³. Notably, both *T. gondii* and *Neospora caninum* can cause congenital infection, while only *T. gondii* can be transmitted between intermediate hosts by oral ingestion of infected tissues⁹, thus bypassing the sexual phase of the life cycle. These flexible features in the *T. gondii* life cycle likely aid in transmission through the food chain, thus underlying its broad host range (Table 1). In contrast to our appreciation of differences in life cycle, modes of transmission and host range among these closely related parasites, their molecular bases remain largely unexplored.

In North America and Europe, the population structure of *T. gondii* is dominated by three prevalent clonal lineages¹⁰, which coexist with much more rare, genetically diverse isolates. A fourth clonal lineage is largely confined to North America, where it is more common in wild animals¹¹. In contrast, much greater genetic diversity is seen in South America where the population lacks signs of the recent genetic bottleneck and clonal structure seen in the Northern Hemisphere¹⁰. *T. gondii* utilizes rodents and birds as natural intermediate hosts, and hence it is particularly well adapted for survival in these niches³. Forward genetic mapping studies have identified several families of secretory proteins in *T. gondii* that are important for thwarting innate immunity and hence facilitating infection in the mouse¹². Related effectors are conserved in *Hammondia hammondi*¹³, hence the basis for the dramatic differences in biology of these two parasites remains unclear. Nonetheless, one hypothesis advanced by the study of select laboratory strains in the mouse model is that pathogenicity, and perhaps host range, may depend on the repertoire of such secretory pathogenicity determinants, although this has not been tested on a wider level.

Here we tested the generality of this hypothesis through genomic analyses of 62 strains of *T. gondii* in comparison to several closely related parasites. Our findings reveal that expansion and diversification of secretory pathogenesis determinants (SPDs), which are often tandemly clustered, is a prominent feature of the genomes of *T. gondii* and related tissue-cyst forming coccidians. Furthermore, patterns of block inheritance, due to recent admixture or selective retention, may underlie specific traits that are shared by related lineages of *T. gondii* containing similar combinations of SPDs. These features define the population structure of *T. gondii* and have implications for the evolution of transmission, host range and pathogenicity.

Results

Comparative genomics of tissue-cyst forming coccidians. We undertook a comparative genomics approach to understand the population diversity of *T. gondii* and its relationship to closely related tissue-cyst forming coccidian parasites. First, we generated additional genomic DNA sequence coverage (~26 × coverage) and RNA-seq data (>1,000 × mean coverage of coding sequence) to improve the assembly and annotation for the reference ME49 strain of *T. gondii* (Table 2). We also generated a whole-genome sequence for *H. hammondi* (~66 × coverage; Table 2) and compared these two closely related parasites to the recently completed genomes of *Sarcocystis neurona*¹⁴ and *N. caninum*¹⁵ (Table 2), which cause economically important diseases in horses and cattle, respectively (Table 1). Finally, to provide insight into genetic variation of *T. gondii* we derived whole-genome sequences for 61 additional isolates that were chosen to span presently known global diversity¹⁶ (Supplementary Data 1). Among the total of 62 *T. gondii* strains, 16 reference strains representing the major haplogroups were sequenced by both 454 (3 and 8 kb paired-end libraries) and Illumina (300 bp paired-end libraries) technologies and the resulting reads were assembled and annotated separately (~47 × average sequence coverage) (Supplementary Table 1). The remaining strains were sequenced using Illumina only (~42 × average sequence coverage) and were aligned to the reference strain ME49 (Supplementary Data 1). Below, we present the comparative analyses of these genomes focusing on three broad themes: (1) comparison of *T. gondii* to the most closely related tissue-cyst forming coccidian parasites, (2) analysis of the core genome of *T. gondii* and how it has diversified and (3) examination of how the global population structure of *T. gondii* has been shaped by local genomic admixture.

We compared the whole-genome sequences from four related tissue-cyst forming coccidian parasites spanning a range of biological hosts and life-cycle strategies (Tables 1 and 2, Fig. 1). Three of the four organisms have a similar total genome size of 62–65 Mb (*N. caninum*, *T. gondii* and *H. hammondi*), while the *S. neurona* genome is somewhat larger due to expanded repeats and much larger introns (Table 2, Supplementary Table 1)¹⁴. All four genomes have roughly similar GC compositions and are predicted to encode from 7,000 to slightly more than 8,000 genes located on 14 chromosomes, as verified in *T. gondii*¹⁷ (Table 2). Similar to other genome sequencing projects, 42–56% of the predicted CDSs (coding DNA sequences) encode genes with a putative functional domain annotation, while 44–58% are hypothetical unknowns. To identify conserved features, we compared the four different genomes to the enteric coccidian *Eimeria tenella*¹⁸ using OrthoMCL to cluster genes into putative orthogroups¹⁹. Not surprisingly, more closely related taxa showed a higher degree of shared OrthoMCL clusters (Fig. 1b, Supplementary Data 2). Orthogroups classified by Pfam²⁰ domains and grouped into the top 20 Gene Ontology

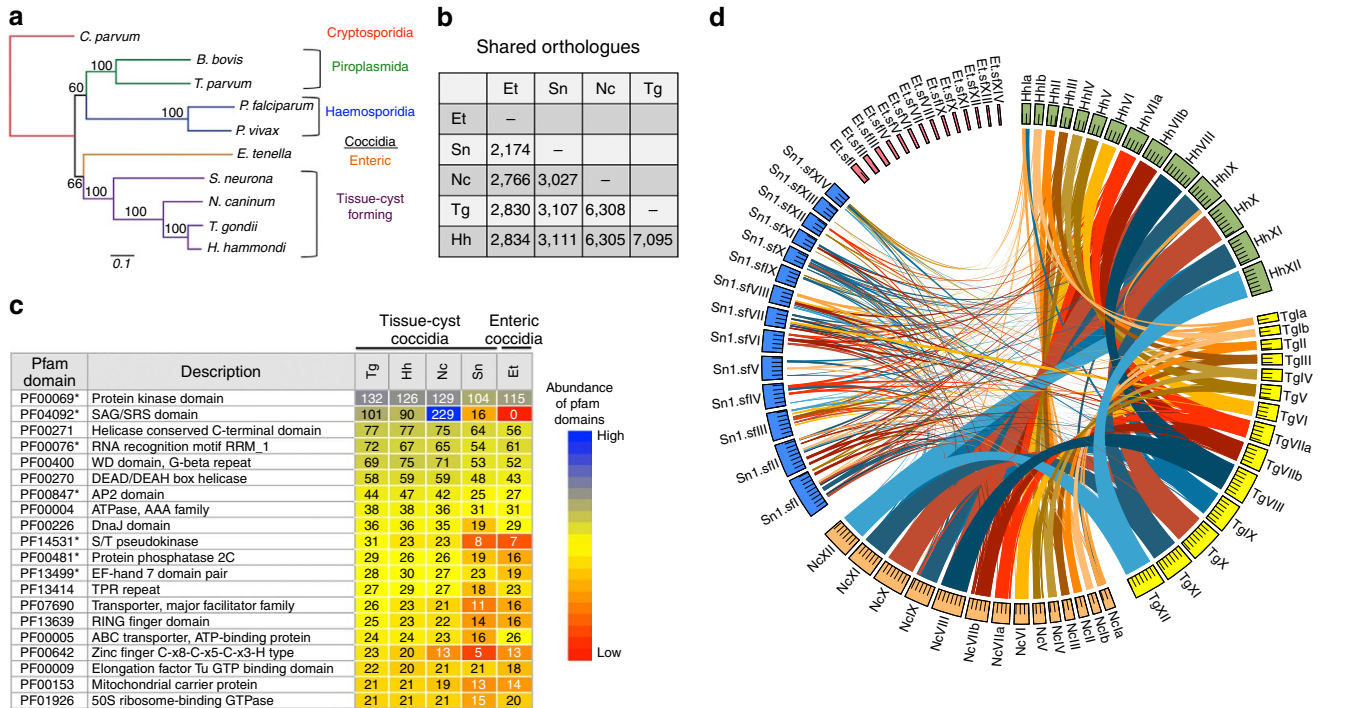


Figure 1 | Comparative genomics of tissue-cyst forming coccidian parasites. (a) Phylogenetic tree of selected apicomplexans based on a conserved DEAD box helicase protein (TGME49_249810, OrthoMCL OG5126701). Neighbour-joining tree with bootstrap values indicated. Distance equals 0.1 amino acid substitutions/site. Taxa names from <http://tolweb.org/Apicomplexa>. (b) Summary of conserved orthologues based on OrthoMCL analysis. Et, *E. tenella*; Hh, *H. hammondi*; Nc, *N. caninum*; Sn, *S. neurona*; Tg, *T. gondii*. (c) Abundance of Pfam domains in coccidian parasites. For each species, the incidence of Pfam domains per protein was determined. The top 20 Pfam domains in *T. gondii* ME49 are shown along with the number of proteins containing these domains in each of the species. The cells in the table are colour coded based on the rank of Pfam domains in terms of their abundance. The domains of interest are indicated by an asterisk. Taxa as in a. (d) Circos plot illustrating levels of synteny among the coccidian parasites. The large outer circle represents the annotated chromosomes or scaffolds of each coccidian species. For *T. gondii*, *H. hammondi* and *N. caninum* all assembled chromosomes ($n=14$) are plotted. For *S. neurona* and *E. tenella*, the largest 14 scaffolds are plotted. Each chromosome/scaffold is labelled with the genus-species abbreviation followed by the chromosome/scaffold number. Tick marks on the chromosome/scaffold represent 1 Mb. The coloured bands and lines linking chromosome/scaffold pairs represent syntenic blocks (minimum of three genes) shared by the chromosomes that are connected. The syntenic links are drawn with *T. gondii*, *H. hammondi* and *N. caninum* as the reference, in that order. Syntenic blocks were generated using genes present in orthologue clusters, where the cluster contained at least one gene from each species.

Table 1 | Summary of the life cycle, host range and pathogenicity of tissue-cyst forming coccidian parasites.

Organism	Definitive host	Alternative host(s)	Transmission	Animal disease	Human disease
<i>Sarcocystis neurona</i>	Opossum	Skunk, raccoon and other small mammals	Obligatory sexual-asexual cycle	Myeloencephalitis in horses and marine mammals	None
<i>Neospora caninum</i>	Canine	Bovine	Vertical asexual or sexual-asexual cycle	Congenital, abortion in cattle neurological, paralysis in dogs	None
<i>Hammondia hammondi</i>	Feline	Rodents	Obligatory sexual-asexual cycle	None	None
<i>Toxoplasma gondii</i>	Feline	Warm-blooded vertebrates	Vertical asexual, sexual-asexual cycle or direct asexual transmission	Congenital, abortion in sheep	Opportunistic pathogen in humans; CNS, ocular, congenital

(GO) terms (<http://geneontology.org/>) revealed that all five species share similar orthologous groups for many key biological functions, and that tissue-cyst coccidians are enriched in processes involved in protein modification (Supplementary Fig. 1).

The most abundant protein domains in tissue-cyst forming coccidian parasites include serine/threonine (S/T) kinases,

RNA-binding proteins, PP2C-type S/T phosphatases and calcium-binding motifs (EF-hands) (Fig. 1c). There is a precedent for the importance of S/T kinases²¹, such as the expanded polymorphic family of rhoptyr (ROP) kinase virulence determinants in *T. gondii*¹² and of calcium-binding motifs, including within a family of calcium-dependent protein kinases²². However, the abundance of RNA-binding proteins (RMR and

Table 2 | Summary of genome features for *T. gondii* and representative apicomplexans.

Feature	<i>S. neurona</i> [*]	<i>N. caninum</i> [†]	<i>H. hammondi</i> [‡]	<i>T. gondii</i> ME49 [§]
Estimated size	~127 Mb [*]	~62 Mb [†]	~65 Mb	~65 Mb
Assembly length without sequencing gaps (bp)	117,871,271	57,524,119	67,460,985	65,464,221
Number of scaffolds	116	NA [†]	99	47
Scaffolds N50 (bp)	2,890,735	NA	1,494,935	6,301,488
Number of contigs [#]	8,903	241	1,337	410
Contigs N50 (bp)	20,915	405,161	84,429	1,219,553
Sequencing depth	375 ×	8 × [†]	66 ×	26.5 ×
# Chromosomes	NA	14 [†]	14	14
# Protein-coding genes	7,093	6,936 ^{**}	8,004 [‡]	8,322 [§]
GC content	51.5%	54.8%	52.5%	52.2%
% Protein-coding sequence ^{††}	50.9%	59%	57.3%	60.5%
Average length of protein-coding genes ^{‡‡} (bp)	9,121	4,892	4,868	4,778
Average number of exons per protein-coding gene	5.5	12	11.7	11.5

NA, not available.

^{*}All sequence reads were deposited in the National Center for Biotechnology (NCBI) sequence read archive under accession SUB554996 ref. 14.[†]Reid et al.¹⁵.[‡]GenBank Assembly ID GCA_000258005.2.[§]GenBank Assembly ID GCA_000006565.2.^{||}Scaffolds >10,000 bp.[#]960 Scaffolds, any size.[#]Contigs >2,000 bp.^{**}GenBank Assembly ID GCA_000208865.2.^{††}Exons and introns, without UTRs.^{‡‡}Without UTRs.

RMA motifs) was unexpected, as these have been largely unexplored in *T. gondii* and closely related parasites. In addition, plant-like AP2 transcription factors are abundant in tissue-cyst forming coccidian parasites (Fig. 1c), consistent with these being major transcription factors in apicomplexans²³. Also prevalent in *N. caninum*, *T. gondii* and *H. hammondi* are a family of surface antigens (SAG) called the SRS family (Fig. 1c), which are amplified and highly divergent among tissue-cyst forming coccidian parasites²⁴. These appear less abundant in *S. neurona* and absent in *E. tenella* (Fig. 1c), although this result is likely due to their divergence from canonical SRS domains, as similar families of 6-Cys rich proteins occur in other coccidian parasites¹⁸ and a related family is found in *Plasmodium*²⁵. SRS proteins and related 6-Cys proteins share a common extracellular structural domain²⁶, are typically GPI-anchored, and are thought to play diverse roles in cell attachment, invasion and development.

From the predicted proteomes, we also reconstructed common metabolic pathways, which were highly conserved across *T. gondii*, *H. hammondi* and *N. caninum*, as noted previously¹⁵. Expanding this analysis to include the 16 reference strains of *T. gondii* identified paralogues for certain functions, for example, in the pyrimidine and purine metabolic pathways and fatty-acid biosynthesis (Supplementary Fig. 2). Most enzymes involved in energy metabolism were well conserved with few paralogues and/or non-synonymous polymorphisms. Previous studies have established the ability of these pathways to mediate strain-specific growth differences²⁷. It is therefore interesting to note that several enzymes with the capacity to modulate flux within these pathways were associated with paralogous expansions and/or significant numbers of non-synonymous polymorphisms (Supplementary Fig. 2, Supplementary Data 3).

Finally, we compared the position of genes across the chromosomes to establish the extent of synteny (Fig. 1d, Supplementary Fig. 3, Supplementary Table 2). There was a high degree of conservation of chromosomal position of orthologous genes between *T. gondii* and *H. hammondi*, and this only slightly decreased when they were compared with *N. caninum*, as previously reported for comparisons of *T. gondii* and *N. caninum*^{15,28} (Fig. 1a). Analysis of the more complete

H. hammondi genome provided here revealed that it shares 29 long syntenic blocks with *T. gondii* harbouring >80% of its genes, with only a few blocks rearranged, most notably a ~1 Mb reciprocal translocation between chromosomes Ia and IX (Fig. 1d). In contrast, synteny broke down substantially when these three organisms were compared with *S. neurona* and was completely absent when compared with *E. tenella*, as has been described previously for a pairwise comparison of *T. gondii* and *E. tenella*¹⁸ (Fig. 1d). The loss of synteny since the divergence of enteric from tissue-cyst forming coccidians stands in stark contrast to the conservation of synteny in the kinetoplastidae, fungi and chordates, all groups with greater evolutionary divergence times relative to the coccidians²⁸.

Expanded SPDs in *T. gondii*. To highlight key features of the *T. gondii* genome we depicted the coding capacity of the reference ME49 strain as a Circos plot, where the outermost circle indicates the genes encoded by each of the 14 chromosomes (Fig. 2a, Supplementary Fig. 4). By comparing the average sequence read depth across the genome, we identified chromosomal genes with copy-number variation (CNV) (Fig. 2a, second innermost circle). Expanding this analysis to all 62 strains revealed 14 genes that have evidence of CNV in all strains, and 39 genes with CNV in 90% of the strains (Supplementary Fig. 5, Supplementary Data 4). Examination of patterns of CNV also revealed several examples of large segmental duplications or aneuploidy in specific strains (Supplementary Fig. 6), similar to reports from previous genetic crosses^{29,30}. These regions were genetically homogeneous suggesting they arose by duplication events and are not hybrids created by unequal crossing over at meiosis. The significance of these diploid regions is uncertain, although recent studies in yeast indicate that aneuploidy can accelerate evolutionary adaptation³¹.

Recent comparisons of the draft genomes of *T. gondii* and *H. hammondi*, and the published genome of *N. caninum*, highlighted the expansion of gene families that differ between these otherwise closely related species^{15,32}. Using the newly annotated assembly of the ME49 genome obtained here, and data from 61 additional genomes of *T. gondii*, we expanded these analyses to examine the distribution of amplified genes,

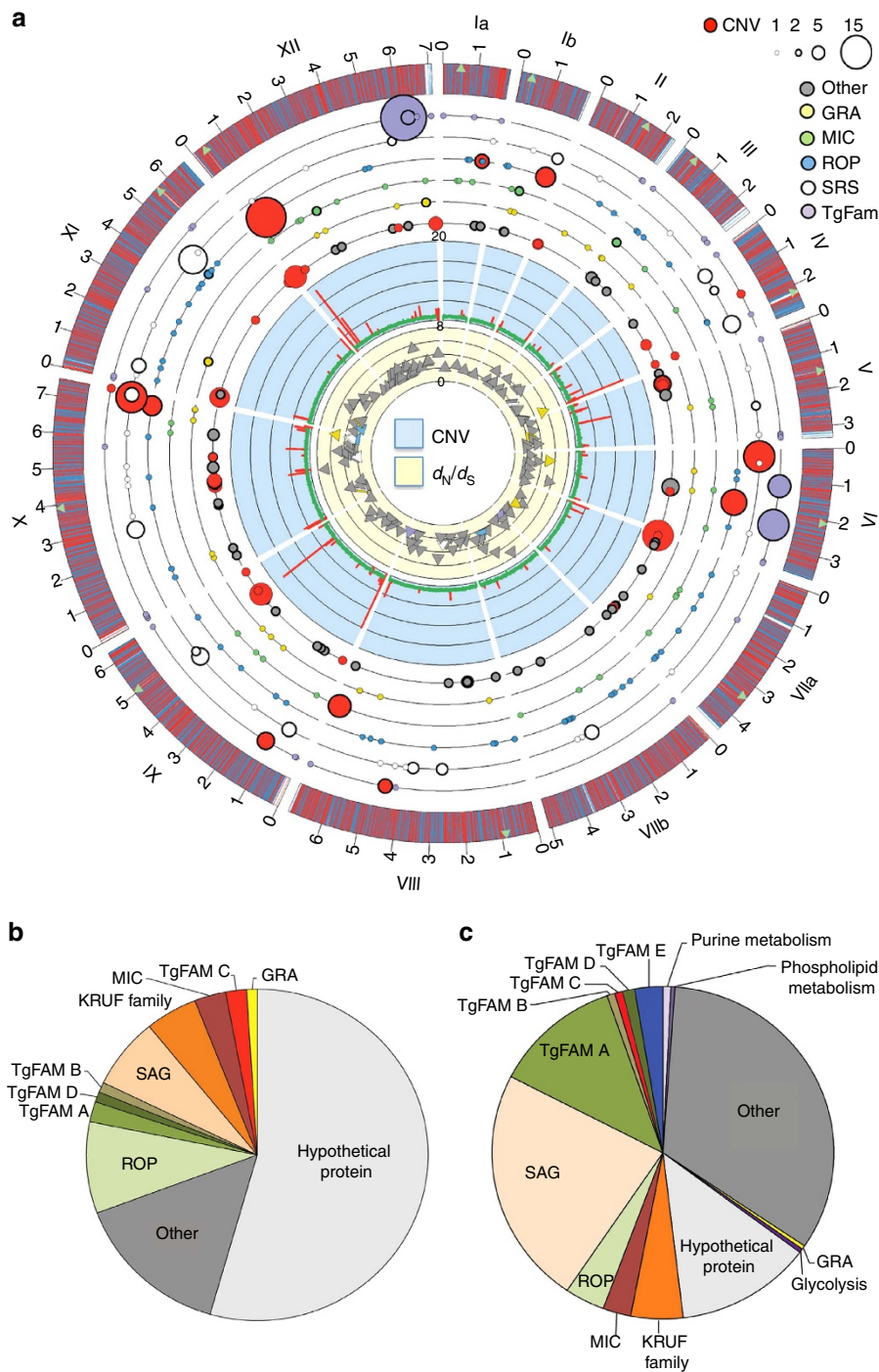


Figure 2 | Composition of the *T. gondii* genome. (a) Circos representational plot of the *T. gondii* genome based on the reference strain ME49. The outside track plots the position of genes on the 14 chromosomes (numbered outside in Roman numerals with size intervals given in Arabic numerals): top strand gene (blue), bottom strand gene (red), centromere locations (green triangles). The innermost track with yellow background is a scatter plot of genes with d_N/d_S ratio ≥ 2 (136 genes): y axis 0-8, colours indicate gene family. The second innermost track with blue background is a histogram of regions with copy number variation (CNV) in ME49 using a rolling window of 2,500 bp: y axis 0-20, 1X copy level (green), region with CNV (red). The next six circular tracks indicate gene families with tandem duplicates or CNV. From the inside to outside, these six levels represent the following categories: other (grey), GRA (yellow), MIC (green), ROP (blue), SRS (white) and TgFAM (purple) genes. The size of the circle is relative to the number of genes (range 1-15). Circles with a thick border indicate tandem arrays while red circles indicate CNV. (b) Frequency of different gene families among genes with CNV includes SPDs such as SAG, ROP, MIC as well as TgFAM genes. (c) Frequency of different gene families among genes with tandem duplications in the assembled genomes includes SPDs such as SAG, ROP, MIC and TgFAM genes.

evident either as CNV or tandem arrays in the assemblies. These amplified genes were plotted as concentric coloured circles corresponding to the protein families they belong to and using

symbols proportional to their total copy number (Fig. 2a). Many of these amplified genes encode secretory or surface proteins that have been previously implicated in host pathogenesis, referred to

here as SPDs. These SPDs include genes encoding secretory proteins found in micronemes (MICs), dense granules (GRA), ROPs, as well as the SRS super family (Fig. 2a, Supplementary Fig. 4). Members of these protein families are known to mediate host cell attachment (MICs)³³, modification of host immunity (GRA and ROP proteins)¹² or adherence and immune evasion (SRS)²⁴. Within the ME49 reference genome, we detected a total of 57 gene loci with CNV, which contain 176 gene copies, and 95 loci in tandem arrays, which contain 264 gene copies (Supplementary Data 4). Both CNV and tandemly duplicated genes were enriched in SPDs, in particular in genes encoding SAG/SRS, ROP and MICs (Fig. 2b,c, Supplementary Data 4), a pattern also noted previously³². For example, SPDs comprised 52 (35%) of the 152 expanded loci and 196 (45%) of the 440

expanded gene copies, despite making up only 375 (4.5%) of the 8,311 total genes in the ME49 genome. Many of the SPDs also show evidence of positive selection, evident in elevated frequencies of non-synonymous (d_N) versus synonymous (d_S) mutations (Fig. 3a). Among these, the *GRA*, *ROP* and *SAG* genes show some of the highest levels of d_N/d_S , while metabolic enzymes typically show selection for conservation, as seen by low levels of d_N/d_S (Fig. 3a, Supplementary Data 5).

We expanded the analysis of SPDs to examine their diversity among a set of reference genomes representing the 16 major haplogroups (Fig. 3b). OrthoMCL clustering of the SPD families revealed that while most members were represented in all 16 haplogroups, differences in representation and copy number were most evident in the SRS and ROP families (Fig. 3b). Collectively,

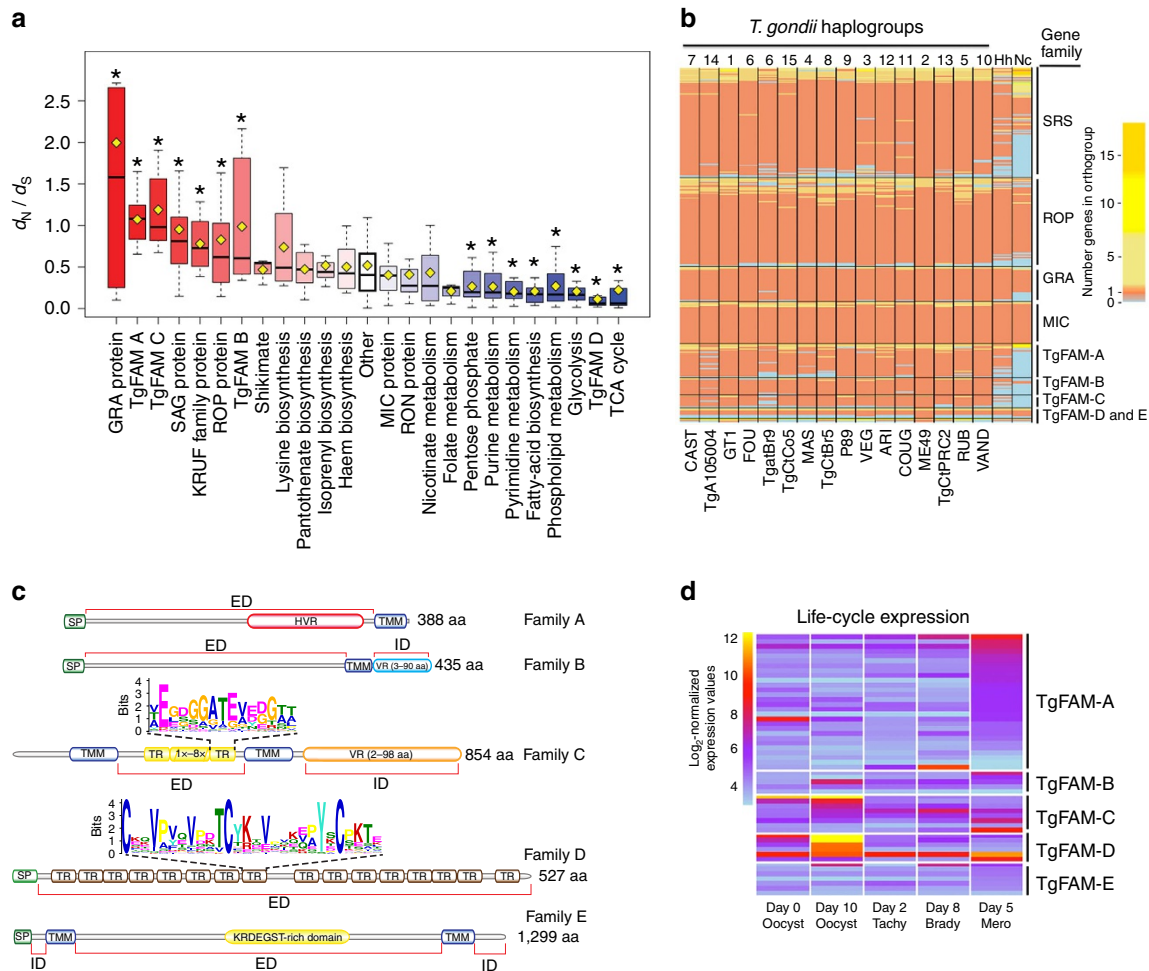


Figure 3 | Analysis of expanded or positively selected gene families in *T. gondii*. (a) Analysis of positive selective pressure among *T. gondii* gene families based on d_N/d_S . Red values indicate categories with significantly elevated d_N/d_S ratios, indicating positive selection for diversification, while blue values indicate categories with significantly reduced values, indicative of selection for conservation. Analysis based on 16 reference *T. gondii* genomes, although similar patterns were also seen for all 62 strains. Horizontal black line d_N/d_S median; yellow square, d_N/d_S mean; mean values significantly different than the category ‘Other’ ($P \leq 0.05$, Mann–Whitney–Wilcoxon test) are denoted with ‘*’. (b) Heatmap of the abundance of SPDs in conserved orthogroups. The number of genes in orthogroups containing SPD genes was determined across the 16 *T. gondii* reference genomes, *H. hammondi* and *N. caninum*, and plotted as a heatmap. Each row is an orthogroup, and the colour of each cell represents the number of genes in that orthogroup, range 0–19. (c) Schematic representation of domain structure of *T. gondii* protein families A to E. Family names and average protein lengths per family are indicated on the right. HVR, hypervariable region; KRDEGST-rich domain, protein domain rich in polar amino acids Lysine (K), Arginine (R), Aspartate (D), Glutamate (E), Serine (S), Threonine (T) and Glycine (G); SP, signal peptide; TMM, transmembrane domain; TR, tandem-repeat domain; VR, protein domain of variable length and sequence. Sequence motifs for each tandem-repeat unit are depicted in Logo format. Extra (ED) and intracellular (ID) protein domains, as predicted by Phobius, are indicated below protein schemes. (d) Life-cycle expression of *TgFAM* genes. Heatmap of \log_2 -normalized microarray expression values for *TgFAM* genes across the *T. gondii* life cycle^{36,66,67}. Background values for the array are near \log_2 of 5. Samples for unsporulated oocysts (Day 0 Oocyst), sporulated oocysts (Day 10 Oocyst), intermediate host tachyzoites (Day 2 Tachy), intermediate host dormant bradyzoite cysts (Day 8 Brady), and enteric stage merozoites (Day 5 Mero) are plotted.

these analyses reveal that the major difference between *T. gondii* strains is the diversification of SPD family members.

Comparison of orthologues for *GRA*, *ROP* and *SRS* genes between *T. gondii*, *H. hammondi* and *N. caninum* revealed substantial differences in clustering by OrthoMCL, suggesting that the divergence among these genes may underlie biological differences between these species (Fig. 3b, Supplementary Fig. 7). In contrast, *MIC* genes were highly conserved, suggesting these organisms use a similar repertoire of host receptors (Fig. 3b). Comparison of OrthoMCL groupings also identified a number of putative species-specific genes unique to *N. caninum*, *H. hammondi* or *T. gondii* (Supplementary Fig. 8a, Supplementary Data 6). Further analysis indicated that a subset of the putative species-specific genes represent distant orthologues that are classified as separate groups by OrthoMCL (Supplementary Fig. 8b, Supplementary Data 6). Notably, this distant orthologue category is greater when comparing *N. caninum* to either *T. gondii* or *H. hammondi*, versus the pairwise comparison between the later two species. Among these distantly related orthologues, a number encode *TgFAM* or *SRS* genes, consistent with the idea that they influence important aspects of the biology (Supplementary Data 6). In contrast, a large number of the genes that differ between *T. gondii* and *H. hammondi* show evidence of alternative gene models, including early truncations, premature stop codons and frame shifts (Supplementary Fig. 8b, Supplementary Data 6). In addition, a smaller number of genes were present only in one species and are predicted to be unique, the majority of which were annotated as hypothetical unknowns. Analysis of alternative allele frequencies, RNA-seq data, and sequencing depth coverage failed to find evidence that these predicted differences are due to sequencing or assembly errors and instead suggest that many are genuine (Supplementary Fig. 8 c–f). Consequently, the putative unique gene list provided in Supplementary Data 6 provides a tentative starting point to identify genes that may mediate important biological differences between these closely related species.

In addition to the previously recognized SPDs, we identified families of genes that are uniquely enriched in the *T. gondii* genome, referred to here as *TgFAM* genes (Fig. 3c, Supplementary Data 7), including one previously referred to as Toxoplasma-specific family (*TSF*¹⁸), which corresponds to *TgFAMC* here. Our analysis of multiple *T. gondii* genomes reveals a much broader set of Toxoplasma-specific families (*TgFAMs*) (Supplementary Data 7), five of which we have specifically highlighted for their unique domain structures (Fig. 3c). Several *TgFAMs* are expanded and show evidence of CNV and/or tandem duplication, while others are located at the ends of chromosomes (Fig. 2), as previously noted for the *TSF* family³⁴. This pattern of telomeric clustering has also previously been associated with antigenic variant surface adhesins in *Plasmodium*³⁵. Although *T. gondii* is not known to undergo antigenic variation, the variable domains of the *TgFAMs* may represent adaptations to enhance host cell recognition and/or escape immune detection. We have highlighted five of the *TgFAMs* here based on the fact that they contain conserved signal peptides as well as domain architectures that suggest they may encode surface proteins with extracellular domains that contain conserved protein motifs (Fig. 3c). *TgFAM* genes are expanded in *T. gondii*, although they are less common in *H. hammondi* and *N. caninum* (Fig. 3b, Supplementary Data 7). In particular, *H. hammondi* and *N. caninum* contain far fewer members of *TgFAMA* and *TgFAMB*, and *TgFAMC* appears to be largely absent in *N. caninum* (Fig. 3b, Supplementary Fig. 7). Notably, many of the *TgFAM* genes highlighted here are expressed during sexual development in the cat gut or in oocysts that are shed into the environment following the sexual phase (Fig. 3d)³⁶, suggesting they may play roles during transmission. In addition to

the *TgFAM* genes highlighted here, there are a number of other gene families containing parasite-specific motifs that are expanded in *T. gondii*, and which may contribute to important biological traits not yet identified (Supplementary Data 7).

Co-inheritance of haploblocks shape population structure.

Previous studies have reported the influence of recombination on the global population structure of *T. gondii*, which shows marked geographic segregation of major haplogroups^{16,37,38}, although the factors shaping these patterns remain unresolved. To examine the population structure based on genome-wide polymorphism data, we analysed single nucleotide polymorphisms (SNPs) that were defined by comparison of 61 *T. gondii* strains to the reference ME49 genome and filtered this set to include positions where reliable data were available for all strains (a total of 802,764 positions in each genome (Supplementary Data 8)). Generation of a neighbour network³⁹ for these data revealed that the 62 strains group closely with haplogroups and major clades that were previously defined by lower resolution genotyping (Fig. 4a)¹⁶. Importantly, similar groupings were defined using admixture⁴⁰ (Supplementary Fig. 9) and principal components analysis (Supplementary Fig. 10). Collectively, these findings support a population structure consisting of a small number of clades that show strong geographic segregation, as described previously^{16,37}.

Although the neighbour network permits visualization of gene flow along several pathways, it does not fully capture the extent or pattern of local genomic admixture among any given pair of strains. To illustrate this more directly, we generated pairwise SNP diversity plots for three of the haplogroups contained in clade D, comparing them to the reference strain ME49 (Fig. 4b). Strains like ARI (haplogroup 12), a sister group of type 2 that is also found in North America, contain large haploblocks that are similar to ME49 (~60%), interspersed with regions that are divergent (Fig. 4b), consistent with previous findings that these two groups are closely related¹¹. In contrast, *TgCtPRC2* (haplogroup 13), which is a common clonal genotype in China⁴¹, shares fewer regions with ME49 (~40%) and COUG (haplogroup 11), which represents a rare North American lineage found in wild animals, showed almost no conserved regions with ME49 (<1%) (Fig. 4b). Thus although members of a common clade contain distinct genomic patterns that have arisen by different evolutionary paths, it is striking that many share large conserved haploblocks across their genomes.

To better represent the shared ancestry across strains, we analysed local inheritance patterns using chromosome painting to reveal patterns of local admixture. When strains were aligned by clade, the presence of shared haploblocks across members was evident by common colour patterns (Fig. 4c, Supplementary Fig. 11). These shared regions represent chromosomal haploblocks that show a high degree of shared ancestry, in some cases eroding the boundaries of the clade structure. Noteworthy, this analysis also revealed patterns of local admixture that suggest the occurrence of genetic crosses among strains of different clades, likely favoured by their geographic proximity (Fig. 4c, Supplementary Fig. 11). Similar shared chromosomal haploblocks are also seen in average pairwise plots for SNPs among members of individual clades (Supplementary Fig. 12). Among the most strongly conserved haploblocks is chromosome Ia, which is shared across nearly all clades, with the exception of clades E and F (Fig. 4c,d, Supplementary Fig. 13). The basis for the widespread conservation of chromosome Ia (ref. 37) is uncertain, but recent studies suggest that it may be due to the enhanced transmission in domestic cats⁴².

The analyses presented above suggest that common inheritance of large haploblocks is the major factor in determining the phylogenetic grouping of *T. gondii* strains. To test this model, we

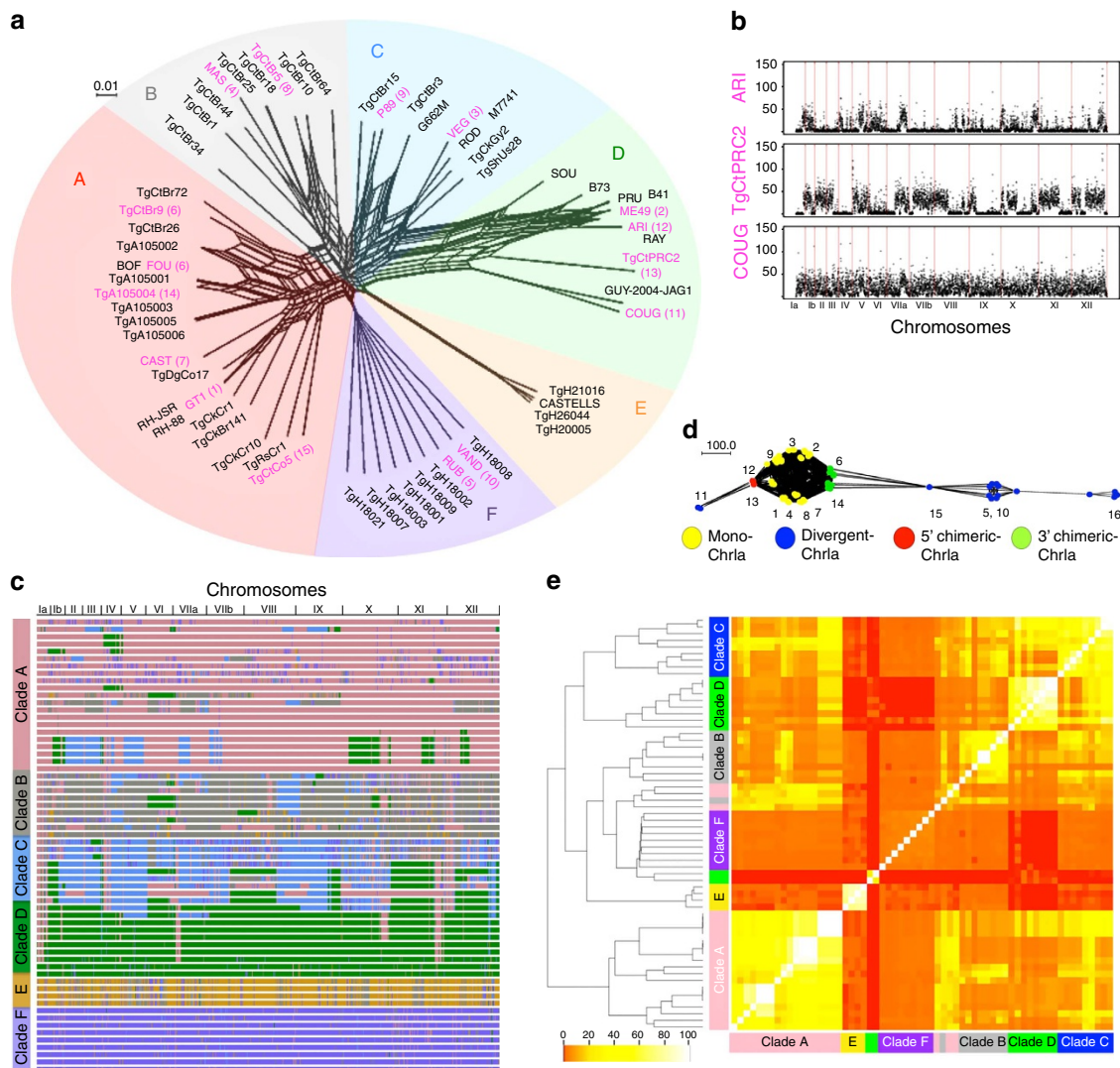


Figure 4 | Comparative genomics and population structure of *T. gondii*. (a) Population genetic structure of *T. gondii*. Neighbour-net analysis based on genome-wide SNPs (802,764 common data points) from 62 isolates of *T. gondii*. Colour wheel indicates major clades of *T. gondii*. Haplogroup numbers are indicated within parenthesis based on previous designation. Pink names denote the representative strains. Scale bar, number of SNPs per site. (b) Pairwise comparison of SNPs between indicated strains to ME49 shown across 14 chromosomes. y axis = number of SNPs/10 kb window. (c) Chromosome painting of 62 *T. gondii* strains. Local admixture analyses were conducted on SNP blocks of size 1,000 on each of the 14 chromosomes. For each SNP block, local admixture was used to assign strains to a particular ancestral population. The shared inheritance of blocks across members reveals colour patterns that extend vertically in the plot. For example, several pink regions show strong vertical patterns bifurcating across multiple clades, although the dominant colour is not meant to imply origin. (d) Network of chromosome 1a (Chr1a) showing high conservation within most haplogroups (number) and clades. Monomorphic forms (Mono, 3' Chimeric, 5' Chimeric) are shared by most lineages, while a few strains are highly divergent. Scale bar, total number of changes. (e) Heatmap clustering of co-inheritance of shared blocks. The percentage of shared blocks between two strains was determined for all 62 x 62 pairwise strain comparisons (1,953 non-redundant comparisons): Scale bar, % shared blocks. Hierarchical clustering on percent shared blocks independently grouped the strains by clade.

performed two types of analysis to cluster strains using the SNP data. First, we analysed SNPs using the linkage model of ChromoPainter in FineStructure⁴³ to generate a clustering hierarchy. This model, which combines information across linked markers in a co-ancestry matrix, recreated the clades seen in the previous analysis with several minor exceptions (Supplementary Fig. 14). Separately, we analysed the SNPs using a rolling window method to define an overall similarity index based on how many regions were co-inherited between all pairwise comparisons (1,953 unique comparisons), which produced a highly similar clade structure (Fig. 4e, Supplementary Fig. 15). These analyses reveal that the current population structure is defined by recent genomic admixture,

where large chromosomal haploblocks have been inherited in common by members of individual clades. Although recent admixture had previously been suggested by analysing individual regions separately³⁸, the present genome-wide analysis of SNPs establishes that this pattern is a defining feature of the population structure of *T. gondii*.

To further examine the pattern of long-haploblock inheritance, we compared the ancestry of regions that were conserved with those that were more variable. When SNP diversity was averaged for members of the same clade, it emerged that discrete regions of the genome show very low SNP diversity, while others are highly variable (Fig. 5a). Regions of low average pairwise SNP diversity were observed in all clades, but differed in their frequency and

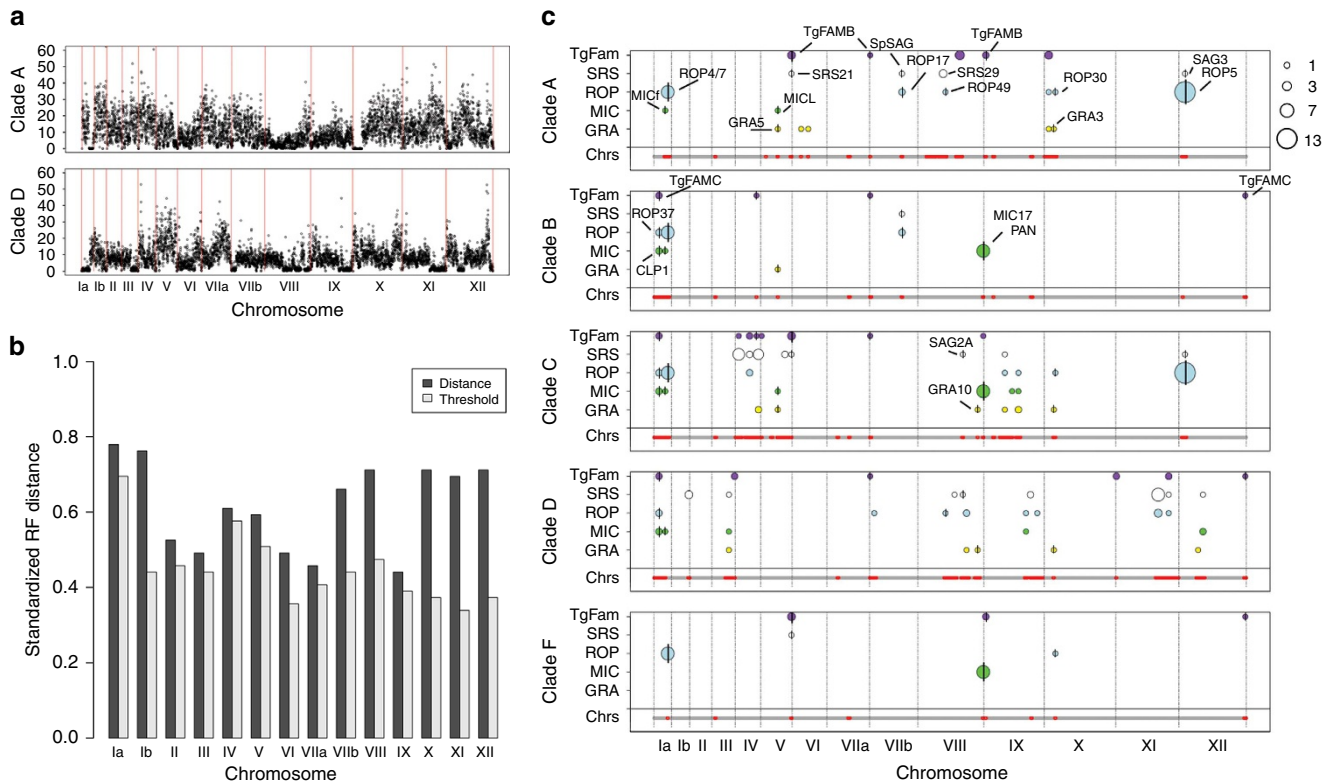


Figure 5 | Analysis of conserved regions within and between clades. (a) Average number of pairwise SNPs that are shared by members of clade A and clade D, y axis 0–60 (outliers >60 not plotted). Each data point represents the average per 10 kb window. Red lines indicate chromosome boundaries. (b) Standardized Robinson-Foulds (RF) distances between phylogenetic trees for conserved and non-conserved regions of the genome, based on average pairwise SNP diversity within each clade compared by maximum likelihood. The standardized RF distance equals the proportion of negative branches between the two trees. Threshold distances for statistical significance ($P \leq 0.002$ per chromosome or ≤ 0.028 for genome wide) were based on 500 bootstrap trees that were used to establish the variation in tree estimates (the height of the threshold bar represents the 99.998% confidence interval of the tree distance). (c) Distribution of conserved regions shared by clades. Horizontal bars below each clade represent the SNP diversity along the combined chromosomes (Chrs). The bar is divided into conserved regions, where the average pairwise SNP diversity is low (red, ≤ 3 SNPs per 10 kb window), versus non-conserved regions where the SNP diversity is high (grey, > 3 SNPs per 10 kb window) based on average pairwise comparisons. Above the bar, the distribution of SPDs within conserved regions for each clade are shown as different colour circles for each gene family: *TgFAM* (purple), *SRS* (white), *ROP* (blue), *MIC* (green) and *GRA* (yellow). Circle sizes are proportional to the number of genes, reflecting tandem clusters or CNV. SPDs that are shared across more than one clade contain a vertical black line and the names are shown in the top-most clade in which they occur. Grey lines indicate chromosome boundaries.

location (Supplementary Fig. 12). To compare the ancestry of different regions of the genomes, we partitioned the genome into two segments based on regions that exhibited low SNP diversity in at least one clade (defined as the union of all regions that were ‘conserved’ in at least one clade) versus regions that showed high SNP diversity in all clades (defined as ‘non-conserved’) (Supplementary Data 9 and 10). We then compared unrooted phylogenetic trees for the conserved versus non-conserved regions using a Robinson–Foulds distance metric, which measures the degree of difference, or distance, between the two sets of trees. This analysis revealed that the ancestry of the conserved haploblocks was significantly different than that of the non-conserved regions for all 14 chromosomes (Fig. 5b). In addition, we generated neighbour networks based on the conserved versus non-conserved regions (Supplementary Fig. 16). The conserved region network most closely resembled the total SNP network (Fig. 4a) and the network based on the non-conserved regions grouped most strains in similar clades, with several notable exceptions (Supplementary Fig. 16). These findings illustrate the importance of the conserved blocks in influencing the grouping of genotypes into clades.

To determine the influence of these shared haploblocks on the content of genes found within specific clades, we plotted the

distribution of SPDs found within conserved regions shared by members of specific clades (Fig. 5c, Supplementary Data 11). The distribution of SPDs revealed that a number of known pathogenicity determinants were common to conserved regions in specific clades (Fig. 5c). We tested whether these patterns were random, or if they showed specific enrichment of SPDs within conserved regions. When clades A, B, C, D and F were analysed together, the pattern of clustering of SPDs was highly significant ($P \leq 0.005$) allowing us to reject the null hypothesis that they were randomly distributed across the genome. SPDs were also significantly clustered in conserved regions when separately analysing clade C ($P \leq 0.005$), clade D ($P \leq 0.05$), and clade F ($P \leq 0.000001$), while clade B was suggestive ($P \leq 0.08$) and clade A was not significant ($P \leq 0.2$). The failure to observe a significant clustering of SPDs in clade A may be due to its considerable substructure that suggests it may actually be comprised of two or more distinct groups. Nonetheless, it is clear that SPDs are often clustered and are found with increased frequency in conserved, shared regions of the genome. SPDs within these regions also share the recent ancestry of the surrounding conserved regions when analysed using phylogenetic trees (Supplementary Figure 17). These findings are consistent with the hypothesis that recent inheritance of conserved blocks

containing specific SPDs is associated with successful expansion of specific lineages and suggest that SPDs impart a selective advantage to members of specific clades.

The co-inheritance of SPDs within conserved regions provides a tentative list of candidates for further study of genes that may underlie important biological traits shared by specific clades. Among these are a number of SPDs previously implicated in acute virulence in the mouse: for example *ROP17* (ref. 44) found in conserved regions in clades A and B, *ROP5* (ref. 29) found in conserved regions in clades A and C, and *GRA3* (ref. 45) found in conserved regions in A, C, D, and F (Fig. 5c). Low diversity regions also contain a number of *SRS* genes, encoding immunologically dominant surface proteins, which have previously been implicated in host cell invasion including sporozoite SAG (Sp-SAG also known as SRS28)⁴⁶ found in conserved regions in clades A and B, SAG3 (SRS57)⁴⁷ found in conserved regions in clades A and C, and SAG2A (SRS34A) (M.E.G., unpublished) found in conserved regions in clades C and D (Fig. 5c, Supplementary Data 11). A second pattern that emerges from this analysis is the presence of clusters of SPDs that are clade-specific, for example clusters of *SRS* and *TgFAM* genes on chromosomes IV, V and IX found in clade C, and clusters of various SPDs on chromosomes II, IX, XI and XII in clade D (Fig. 5c, Supplementary Data 11). Although the specific roles of these genes are unknown, they may underlie common traits that distinguish phenotypes characteristic of specific clades.

Discussion

Toxoplasma gondii belongs to a diverse and ancient phylum of parasites that antedates the wide range of vertebrate hosts that they currently inhabit. It shares a core set of genes and metabolic processes with closely related tissue-cyst forming coccidian parasites. Despite having similar genomic content, these organisms differ dramatically in their host range, pathogenicity and modes of transmission. We demonstrate here that *T. gondii* is demarcated from its closest relatives by the expansion of parasite-specific SPDs that are involved in host–pathogen interactions. Diversification of SPDs also highlights key differences among major clades of *T. gondii*, which are distinguished by common inheritance of large haploblocks in their genomes. Shared inheritance of large haploblocks among related strains reinforces the hypothesis that recombination in the wild, while infrequent, drives important biological adaptations^{48,49}. The distribution of clustered SPDs within conserved regions that show common ancestry identifies a number of candidate genes that may influence both clade specific and more broadly shared traits. Overall, the phenotypic traits of individual strains are likely determined by both their core ancestral genomes, and inheritance of conserved haploblocks, which together comprise their mosaic genomes.

The mosaic genomic patterns seen in specific clades may underlie differences in population structure that exist in different *T. gondii* populations between North and South America¹⁰. Although the common ancestry of conserved blocks among otherwise different genotypes is consistent with recent introgression, the conservation of these regions among members of a given clade may reflect several different mechanisms. Such shared haploblocks may be retained in the face of ongoing recombination in outbreeding populations, suggesting they impart a selective advantage. Alternatively, they may simply reflect recent admixture that has not been eroded due to infrequent recombination, such as in clonal populations. Regardless of their exact histories, strains that inherit conserved haplotype blocks in common will also share clusters of highly related genes, including SPDs that may influence traits such as transmission, host range and pathogenesis.

Expansion of polymorphic genes that are important in pathogenicity is also a key feature of other pathogen genomes. One feature they share in common is that the amplified genes typically encode surface or secretory proteins that interact directly with the host, either to mediate attachment or immune evasion. Examples include: the expansion of surface antigen variants encoded by *VAR* genes in the *Plasmodium falciparum* genome⁵⁰, and the unrelated yet expanded *VIR* genes in *Plasmodium vivax*⁵¹, variant surface glycoprotein encoding genes (*VSG*) in *Trypanosoma brucei*⁵², and the expansion of RXLR effectors in oomycetes⁵³. It is noteworthy that while gene expansion and diversification are common to each of these examples, the protein families involved are largely distinct and reflect the specialized biology of these diverse pathogens. This pattern suggests that expansion of polymorphic gene families is a common theme that underlies important changes in host range and transmission that characterize the evolution of pathogens in their diverse hosts.

Methods

Propagation of strains and isolation of gDNA. Sixty-two representative strains of *T. gondii* were selected from different haplogroups from around the world (Supplementary Data 1)¹⁶. Strains were cultured in human foreskin fibroblast cells, as described previously¹⁶.

Genome sequencing of *T. gondii* reference strains. Sequencing of 16 reference strains of *T. gondii*, and of one isolate of *H. hammondi*, was conducted using a combination of 454, and Illumina PE sequencing technologies (Supplementary Table 1). Sequence reads were screened for contamination and reassembled using Celera Assembler software⁵⁴ or Newbler v2.6 (ref. 54). Scaffolds were then aligned with MUMmer⁵⁵ to *T. gondii* ME49 chromosome sequences from ToxoDB v8.0 (<http://ToxoDB.org>) to generate super-scaffolds spanning entire chromosomes. Annotated genomes were deposited into National Center for Biotechnology (NCBI).

Genome sequencing for SNP discovery. For each of the remaining 46 non-reference strain (Supplementary Data 1), a single Illumina PE barcoded library was prepared from tachyzoite gDNA. Libraries were then pooled into groups of nine samples and sequenced multiplexed in a single lane of an Illumina HiSeq 2000 machine. Sequencing reads were deposited in the Sequence Read Archive repository at NCBI.

Sequencing of tachyzoite messenger RNA samples. To aid in the curation of ME49 gene models, two tachyzoite-specific Illumina complementary DNA libraries were constructed from mRNA isolated from tachyzoite cultures from ME49 and GT1 strains. Each library was then sequenced in a single lane of an Illumina Genome Analyzer II machine.

Structural and functional annotation of the ME49 genome. Gene annotations were derived by comparison of the existing ME49 reference genome (<http://ToxoDB.org>) using a combination of evidence from RNASeq data, cDNA/EST sequences and a variety of software tools to predict potential protein-coding genes using an in-house pipeline at J. Craig Venter Institute (JCVI) (Supplementary Methods). Predicted proteins were run through JCVI's auto-naming pipeline, that assign product names based on a number of sequence similarity searches including blastp searches against the previous *T. gondii* ME49 proteome (ToxoDB v8.0; <http://ToxoDB.org>) and the GenBank non-redundant protein database, HMM searches against Pfam and TIGRFam⁵⁶ databases, and RPS-Blast searches against the NCBI-CDD database⁵⁶. Proteins without any significant hit to other proteins or protein domains were flagged as 'hypothetical protein'. The final list of product names was then curated by researchers from the *Toxoplasma* research community before being assigned to working models. ME49 protein-coding genes were assigned similar pub_locus identifiers to the previous genome assembly while newly predicted protein-coding genes were assigned completely new pub_locus identifiers (Supplementary Methods).

Annotation of *T. gondii* reference strains and *H. hammondi*. Functional annotation of protein-coding genes in other *T. gondii* reference strains was performed as above. Genes syntenic to ME49 inherited their product names, GO terms, and Enzyme Commission numbers, while non-syntenic genes acquired their names and other functional annotations from the output of JCVI's autonaming pipeline. Structural and functional annotations of *H. hammondi* were carried out following a similar approach with slight modifications (Supplementary Methods).

Domain Identification of *T. gondii* novel gene families. To identify known protein domains the *T. gondii* ME49 proteome was searched against Pfam and TIGRFam HMM profiles using HMMER3 (ref. 57). Proteins matching a particular HMM profile were assigned to that domain and remaining peptides searched against each other using blastp to identify potential novel domains. The top five protein families containing novel para domains (TgFAMs A to E) were analysed using Phobius⁵⁸ to identify signal peptides and transmembrane domains. *De novo* identification of conserved protein domains across members of the same gene family was carried out with MEME⁵⁹. Expression levels for the TgFAMs were obtained from *T. gondii* Affymetrix Array data available from NCBI GEO records GSE32427 and GSE51780.

Estimation of d_N/d_S ratios. Coding sequences from each cluster of orthologous genes from the 16 *T. gondii* reference strains were used to estimate d_N/d_S ratios using a modified version of the Bioperl script *bp_pairwise_kaks.pl* (http://search.cpan.org/dist/BioPerl/scripts/utilities/bp_pairwise_kaks.pl).

SNP identification. Illumina reads for each of the 61 other genomes were aligned using Bowtie2—end-to-end⁶⁰ against the ME49 reference genome assembly (release date 23 April 2013), identifying a total of 2,342,433 SNPs across all strains. Positions with informative base calls for all 62 strains were identified, generating a final list of 802,764 SNPs that were used for analysis.

Analysis of orthologous genes. Annotated proteomes were analysed using OrthoMCL v2.0 (ref. 61) to define orthologous groups. Clusters of orthologous groups were functionally annotated using GO Slim terms, which are designed to group the many different GO terms into smaller groups of related processes (<http://geneontology.org/page/go-slim-and-subset-guide>). The proteomes were queried against the Pfam HMM database using HMMER3 to estimate the abundance of Pfam domains.

Mapping metabolic differences. SNPs from the 16 *T. gondii* reference strains that correspond to the 382 proteins in the iCS382 metabolic pathway reconstruction of *T. gondii* ME49 (ref. 27) were downloaded from ToxoDB (<http://www.toxodb.org/toxo-release4-0/home.jsp>).

Network and principal components analyses. Genome-wide SNPs were saved as FASTA files and directly incorporated into SplitsTree v4.4 (ref. 39) to generate unrooted phylogenetic networks using a neighbour-net method and 1,000 bootstrap replicates. Principal components analysis was performed by eigenanalysis of a co-ancestry matrix implemented in fineSTRUCTURE, as described in ref. 43.

Chromosome Ia analysis. SNP data for ChrIa were plotted as a minimum spanning tree using SplitsTree v4.4 (ref. 39) with 2,000 spring-embedded iterations. The 62 strains were clustered into four major groups denoted as monomorphic, divergent, 5'-chimeric and 3'-chimeric chromosome Ia. SNPs present in each cluster were calculated using a custom script over a 10-kb moving window and plotted using Excel.

Admixture analysis. The population genetic structure of *T. gondii* was determined by an unsupervised clustering algorithm, ADMIXTURE⁴⁰ with ancestral clusters set from $k = 1$ through 10. The number of ancestral clusters k was determined by estimating the low cross-validation error (CV error) for different k values using five-fold CV.

Co-ancestry heatmap. We developed a co-ancestry heatmap by using the linkage model of ChromoPainter (<http://www.paintmychromosomes.com>) and fineSTRUCTURE⁴³ based on the genome-wide SNP data. The burn-in and Markov Chain Monte Carlo (MCMC) after the burn-in were run for 10,000 iterations with default settings.

Estimating CNV. For each strain of *T. gondii*, the respective.sra files were used to align reads to the 14 ME49 reference chromosomes using Bowtie2 with the end-to-end option. The read depth per base pair, or read bases (RB), across 8,320 chromosomal-mapped genes was determined using samtools mpileup⁶². Plots were generated in R (<http://www.r-project.org/>). *T. gondii* gene families organized in tandem arrays were identified with an in-house *perl* script.

Analysis of OrthoMCL species-specific genes. Genes found to be specific to *T. gondii*, *H. Hammondii* or *N. caninum* based on OrthoMCL clustering were further analysed using a combination of sequence alignment tools (Supplementary Methods). Genes were classified based on whether they showed a significant 'Blastp hit', showed blastn similarity that was either 'full length' or constituted an 'alternative gene model', or showed no similarity and were 'unique'. Further analysis was done to investigate these differences by RNA-Seq, analysis of

minimum alternative allele frequency and minimum read depth (Supplementary Methods).

Regions of co-inheritance. To determine the extent of recombination and co-inheritance of blocks between strains, low SNP regions (regions of recent co-inheritance or shared blocks) were identified for 10 kb windows for pairwise strain comparisons. A heatmap was generated using the R function heatmap.2 (gplots library (<http://www.r-project.org/>)) with hierarchical clustering on the % shared blocks value. The number of SNPs per 10 kb window were averaged for all strains within a Clade, and chromosomal regions with low SNP density were identified as above using 10 kb windows that had three or fewer SNPs across a continuous stretch of 10 windows (100 kb), allowing for intermittent outliers.

Identification of SPD genes and clustering within the genome. We identified genes that belong to the SPD families (that is, *MIC*, *GRA*, *ROP*, *SRS* and *TgFAM*) based on the annotation of ME49 accounting for CNV in determining the gene number. We then mapped the position of the SPDs onto the assembled ME49 genome and defined those that fell into conserved or non-conserved regions. To determine if gene type was independent of region type we compared the observed frequency of SPDs and non-SPD genes in conserved versus non-conserved regions of the genome using a χ^2 -squared analysis. The null hypothesis was that the distribution would be random, and there would be no difference between observed and expected. A P value of ≤ 0.05 was considered significant cause for rejection of the null hypothesis.

Ancestry of conserved and non-conserved regions. Phylogenetic trees for the conserved and non-conserved regions were constructed using maximum likelihood as implemented in RAxML version 7.3.0 with the GTR + GAMMA model⁶³. Standardized Robinson–Foulds distances⁶⁴ were calculated between the conserved and non-conserved trees based on 500 bootstrap replicates. Trees were considered congruent if they had no conflicting branches with bootstrap support of >95%.

Phylogeny. Phylogenetic trees were constructed for the conserved OrthoMCL OG5_0126701 using the Neighbour-Joining algorithm with 1,000 bootstrap replicates as implemented in Geneious ver. 7.1.5 (<http://www.geneious.com> (ref. 65)) and visualized with FigTree ver. 1.4.0 (<http://tree.bio.ed.ac.uk/software/figtree/>).

Syntenic. The OrthoMCL ortholog clusters (see above) were reformatted to represent each pair found in the cluster outside of self-matches and syntenic blocks were generated between all combinations of genomes as described in ref. 28.

Chromosome painting. Local admixture analyses using an enhanced ADMIXTURE algorithm⁴⁰ was used to assign each of the 62 strains to clusters representing these ancestral states.

Additional methodology. Detailed methods for the above sections can be found in the supplementary methods.

References

- Baldauf, S. L. The deep roots of eukaryotes. *Science* **300**, 1703–1706 (2003).
- Levine, N. D. *The Protozoan Phylum Apicomplexa* (CRC Press, 1988).
- Dubey, J. P. *Toxoplasma*, *Hammondia*, *Besnoitia*, *Sarcocystis*, and other tissue cyst-forming coccidia of man and animals. in *Parasitic Protozoa* (ed. Kreier, J. P.) 101–237 (Academic Press, 1977).
- Berney, C. & Pawlowski, J. A molecular time-scale for eukaryote evolution recalibrated with the continuous microfossil record. *Proc. Biol. Sci.* **273**, 1867–1872 (2006).
- Dubey, J. P. *Toxoplasmosis of Animals and Humans* 313 (CRC Press, 2010).
- Pappas, G., Roussos, N. & Falagas, M. E. Toxoplasmosis snapshots: global status of *Toxoplasma gondii* seroprevalence and implications for pregnancy and congenital toxoplasmosis. *Int. J. Parasitol.* **39**, 1385–1394 (2009).
- Montoya, J. G. & Liesenfeld, O. Toxoplasmosis. *Lancet* **363**, 1965–1976 (2004).
- Weiss, L. M. & Kim, K. *Toxoplasma gondii: The Model Apicomplexan: Perspectives and Methods* 1085 (Academic Press, 2014).
- Su, C. *et al.* Recent expansion of *Toxoplasma* through enhanced oral transmission. *Science* **299**, 414–416 (2003).
- Sibley, L. D. & Ajioka, J. W. Population structure of *Toxoplasma gondii*: Clonal expansion driven by infrequent recombination and selective sweeps. *Annu. Rev. Microbiol.* **62**, 329–351 (2008).
- Khan, A. *et al.* Genetic analyses of atypical *Toxoplasma gondii* strains reveals a fourth clonal lineage in North America. *Int. J. Parasitol.* **41**, 645–655 (2011).
- Hunter, C. A. & Sibley, L. D. Modulation of innate immunity by *Toxoplasma gondii* virulence effectors. *Nat. Rev. Microbiol.* **10**, 766–778 (2012).
- Walzer, K. A. *et al.* *Hammondia hammondi*, an avirulent relative of *Toxoplasma gondii*, has functional orthologs of known *T. gondii* virulence genes. *Proc. Natl Acad. Sci. USA* **110**, 7446–7451 (2013).

14. Blazejewski, T. *et al.* Systems based analysis of the *Sarcocystis neurona* genome identifies pathways that contribute to a heteroxenous life cycle. *MBio* **6**, 02445–14 (2015).
15. Reid, A. J. *et al.* Comparative genomics of the apicomplexan parasites *Toxoplasma gondii* and *Neospora caninum*: coccidia differing in host range and transmission strategy. *PLoS Pathog.* **8**, e1002567 (2012).
16. Su, C. L. *et al.* Globally diverse *Toxoplasma gondii* isolates comprise six major clades originating from a small number of distinct ancestral lineages. *Proc. Natl Acad. Sci. USA* **109**, 5844–5849 (2012).
17. Khan, A. *et al.* Composite genome map and recombination parameters derived from three archetypal lineages of *Toxoplasma gondii*. *Nucleic Acids Res.* **33**, 2980–2992 (2005).
18. Reid, A. J. *et al.* Genomic analysis of the causative agents of coccidiosis in domestic chickens. *Genome Res.* **24**, 1676–1685 (2014).
19. Chen, F., Mackey, A. J., Stoeckert, Jr C. J. & Roos, D. S. OrthoMCL-DB: Querying a comprehensive multi-species collection of ortholog groups. *Nucleic Acids Res* **34**, D363–D368 (2006).
20. Sonnhammer, E. L. L., Eddy, S. R. & Durbin, R. Pfam: a comprehensive database of protein families based on seed alignments. *Proteins* **3**, 405–420 (1997).
21. Miranda-Saavedra, D., Gabaldon, T., Barton, G. J., Langsley, G. & Doerig, C. The kinomes of apicomplexan parasites. *Microbes Infect.* **14**, 796–810 (2012).
22. Billker, O., Lourido, S. & Sibley, L. D. Calcium-dependent signaling and kinases in apicomplexan parasites. *Cell Host Microbe* **5**, 612–622 (2009).
23. Balaji, S., Babu, M. M., Iyer, L. M. & Aravind, L. Discovery of the principal specific transcription factors of Apicomplexa and their implication for the evolution of the AP2-integrase DNA binding domains. *Nucleic Acids Res.* **33**, 3994–4006 (2005).
24. Wasmuth, J. D. *et al.* Integrated bioinformatic and targeted deletion analyses of the SRS gene superfamily identify SRS29C as a negative regulator of *Toxoplasma virulence*. *mBio* **3**, e00321–12 (2012).
25. Arredondo, S. A. *et al.* Structure of the *Plasmodium* 6-cysteine s48/45 domain. *Proc. Natl Acad. Sci. USA* **109**, 6692–6697 (2012).
26. Tonkin, M. L. *et al.* Structural and biochemical characterization of *Plasmodium falciparum* 12 (Pf12) reveals a unique interdomain organization and the potential for an antiparallel arrangement with Pf41. *J. Biol. Chem.* **288**, 12805–12817 (2013).
27. Song, C. *et al.* Metabolic reconstruction identifies strain-specific regulation of virulence in *Toxoplasma gondii*. *Mol. Syst. Biol.* **9**, 708 (2013).
28. DeBarry, J. D. & Kissinger, J. C. Jumbled genomes: missing Apicomplexan synteny. *Mol. Biol. Evol.* **28**, 2855–2871 (2011).
29. Behnke, M. S. *et al.* Virulence differences in *Toxoplasma* mediated by amplification of a family of polymorphic pseudokinases. *Proc. Natl Acad. Sci. USA* **108**, 9631–9636 (2011).
30. Taylor, S. *et al.* A secreted serine-threonine kinase determines virulence in the eukaryotic pathogen *Toxoplasma gondii*. *Science* **314**, 1776–1780 (2006).
31. Selmecki, A. M. *et al.* Polyploidy can drive rapid adaptation in yeast. *Nature* **519**, 349–352 (2015).
32. Adomako-Ankomah, Y., Wier, G. M., Borges, A. L., Wand, H. E. & Boyle, J. P. Differential locus expansion distinguishes Toxoplasmatinae species and closely related strains of *Toxoplasma gondii*. *mBio* **5**, e01003–e01013 (2014).
33. Cowper, B., Matthews, S. & Tomley, F. The molecular basis for the distinct host and tissue tropisms of coccidian parasites. *Mol. Biochem. Parasitol.* **186**, 1–10 (2012).
34. Dalmaso, M. C., Carmona, S. J., Angel, S. O. & Agüero, F. Characterization of *Toxoplasma gondii* subtelomeric-like regions: identification of a long-range compositional bias that is also associated with gene-poor regions. *BMC Genomics* **15**, 21 (2014).
35. Scherf, A., Lopez-Rubio, J. J. & Riviere, L. Antigenic variation in *Plasmodium falciparum*. *Annu. Rev. Microbiol.* **62**, 445–470 (2008).
36. Behnke, M. S., Zhang, T. P., Dubey, J. P. & Sibley, L. D. *Toxoplasma gondii* merozoite gene expression analysis with comparison to the life cycle discloses a unique expression state during enteric development. *BMC Genomics* **15**, 350 (2014).
37. Khan, A. *et al.* Recent transcontinental sweep of *Toxoplasma gondii* driven by a single monomorphic chromosome. *Proc. Natl Acad. Sci. USA* **104**, 14872–14877 (2007).
38. Minot, S. *et al.* Admixture and recombination among *Toxoplasma gondii* lineages explain global genome diversity. *Proc. Natl Acad. Sci. USA* **109**, 13458–13463 (2012).
39. Huson, D. H. & Bryant, D. Application of phylogenetic networks in evolutionary studies. *Mol. Biol. Evol.* **23**, 254–267 (2006).
40. Alexander, D. H., Novembre, J. & Lange, K. Fast model-based estimation of ancestry in unrelated individuals. *Genome Res* **19**, 1655–1664 (2009).
41. Zhou, P. *et al.* Genetic characterization of *Toxoplasma gondii* isolates from pigs in China. *J. Parasitol.* **96**, 1027–1029 (2010).
42. Khan, A. *et al.* Geographic separation of domestic and wild strains of *Toxoplasma gondii* in French Guiana correlates with a monomorphic version of chromosome1a. *Plos Negl. Trop. Dis.* **8**, e3182 (2014).
43. Lawson, D. J., Hellenthal, G., Myers, S. & Falush, D. Inference of population structure using dense haplotype data. *PLoS Genet.* **8**, e1002453 (2012).
44. Etheridge, R. D., Alagan, A., Tang, K., Turk, B. E. & Sibley, L. D. ROP18 and ROP17 kinase complexes synergize to control acute virulence of *Toxoplasma* in the mouse. *Cell Host Microbe* **15**, 537–550 (2014).
45. Craver, M. P. & Knoll, L. J. Increased efficiency of homologous recombination in *Toxoplasma gondii* dense granule protein 3 demonstrates that GRA3 is not necessary in cell culture but does contribute to virulence. *Mol. Biochem. Parasitol.* **153**, 149–157 (2007).
46. Radke, J. R. *et al.* Identification of a sporozoite-specific member of the *Toxoplasma* SAG superfamily via genetic complementation. *Mol. Microbiol.* **52**, 93–105 (2004).
47. Dzierzinski, F., Mortuaire, M., Cesbron-Delauw, M. F. & Tomavo, S. Targeted disruption of the glycosylphosphatidylinositol-anchored surface antigen SAG3 gene in *Toxoplasma gondii* decreases host cell adhesion and drastically reduces virulence in mice. *Mol. Microbiol.* **37**, 574–582 (2000).
48. Boyle, J. P. *et al.* Just one cross appears capable of dramatically altering the population biology of a eukaryotic pathogen like *Toxoplasma gondii*. *Proc. Natl Acad. Sci. USA* **103**, 10514–10519 (2006).
49. Wendte, J. M. *et al.* Self-mating in the definitive host potentiates clonal outbreaks of the apicomplexan parasites *Sarcocystis neurona* and *Toxoplasma gondii*. *PLoS Genet.* **6**, e1001261 (2010).
50. Gardner, M. J. *et al.* Genome sequence of the human malaria parasite *Plasmodium falciparum*. *Nature* **419**, 498–511 (2002).
51. Carlton, J. M. *et al.* Comparative genomics of the neglected human malaria parasite *Plasmodium vivax*. *Nature* **455**, 757–763 (2008).
52. Berriman, M. *et al.* The genome of the African trypanosome *Trypanosoma brucei*. *Science* **309**, 416–422 (2005).
53. Baxter, L. *et al.* Signatures of adaptation to obligate biotrophy in the *Hyaloperonospora arabidopsidis* genome. *Science* **330**, 1549–1551 (2010).
54. Miller, J. R., Koren, S. & Sutton, G. Assembly algorithms for next-generation sequencing data. *Genomics* **95**, 315–327 (2010).
55. Delcher, A. L., Phillippy, A., Carlton, J. & Salzberg, S. L. Fast algorithms for large-scale genome alignment and comparison. *Nucleic Acids Res.* **30**, 2478–2483 (2002).
56. Marchler-Bauer, A. *et al.* CDD: conserved domains and protein three-dimensional structure. *Nucleic Acids Res.* **41**, D348–D352 (2013).
57. Eddy, S. R. Accelerated Profile HMM Searches. *PLoS Comput. Biol.* **7**, e1002195 (2011).
58. Kall, L., Krogh, A. & Sonnhammer, E. L. A combined transmembrane topology and signal peptide prediction method. *J. Mol. Biol.* **338**, 1027–1036 (2004).
59. Bailey, T. L. *et al.* MEME SUITE: tools for motif discovery and searching. *Nucleic Acids Res.* **37**, W202–W208 (2009).
60. Langmead, B. & Salzberg, S. L. Fast gapped-read alignment with Bowtie 2. *Nat. Methods* **9**, 357–359 (2012).
61. Li, L., Stoeckert, Jr C. J. & Roos, D. S. OrthoMCL: identification of ortholog groups for eukaryotic genomes. *Genome Res.* **13**, 2178–2189 (2003).
62. Li, H. *et al.* The Sequence Alignment/Map format and SAMtools. *Bioinformatics.* **25**, 2078–2079 (2009).
63. Stamatakis, A. RAXML-VI-HPC: maximum likelihood-based phylogenetic analyses with thousands of taxa and mixed models. *Bioinformatics.* **22**, 2688–2690 (2006).
64. Robinson, D. R. & Foulds, L. R. Comparison of phylogenetic trees. *Math. Biosci.* **53**, 131–147 (1981).
65. Kearse, M. *et al.* Geneious Basic: an integrated and extendable desktop software platform for the organization and analysis of sequence data. *Bioinformatics.* **28**, 1647–1649 (2012).
66. Buchholz, K. R. *et al.* Identification of tissue cyst wall components by transcriptome analysis of in vivo and in vitro *Toxoplasma gondii* bradyzoites. *Eukaryot. Cell* **10**, 1637–1647 (2011).
67. Fritz, H. M. *et al.* Transcriptomic analysis of toxoplasma development reveals many novel functions and structures specific to sporozoites and oocysts. *PLoS ONE* **7**, e29998 (2012).

Acknowledgements

Sequencing, assembly and annotation for the Tg and Hh genomes reported here were supported by the National Institute of Allergy and Infectious Diseases (NIAID), National Institutes of Health (NIH), Department of Health and Human Services under contract number HHSN272200900007C. Additional analyses were provided by community-based efforts and included support from NIH grants AI059176 and AI036629 (L.D.S.) and the Canadian Institutes for Health Research grant MOP 84556 (J.P.). Data for the Sn annotation was generously provided by M.E.G. and J.P. prior to publication and was supported by the Intramural Research Program of NIAID at the NIH (M.E.G.). Additional computing resources were provided by the SciNet HPC Consortium. We acknowledge ToxoDB (<http://toxodb.org/>) for providing a publically available repository for all genomic data described here and for assistance in coordinating this study. OrthoMCL and ToxoDB are supported in part with funds from the NIAID, NIH, and Department of Health and Human Services under contract HHSN272201400030C (D.S.R. & J.C.K.).

Author contributions

H.L., M.H. and S.K. performed genome assembly and/or annotation; H.L., A.K., M.S.B., S.N., L.S.S., D.P., B.P.B., M.A.D.-M., B.D.G., L.L. and J.C.K. generated data files for analyses; H.L., A.K., M.S.B., S.N., L.S.S., D.K.H., M.E.G., J.P., L.L., J.C.K., D.S.R. and L.D.S. analysed data and generated Figures or Tables; D.A., M.L.D., J.P.D., H.M.F., S.M.G., M.E.G., C.S. and X.Q.Z. provided key biological materials or data; J.W.A., J.P.B., J.C.B., M.E.G., D.K.H., K.K., B.M.R., M.W.W., J.P., J.C.K., J.P.J.S., D.S.R. and L.D.S. provided advice on project design and analyses; H.L., J.P., J.C.K., D.S.R. and L.D.S. supervised the project; H.L., M.S.B., B.M.R., J.P., L.L., J.C.K. and L.D.S. wrote the paper, with input from all authors.

Additional information

Accession codes: Assembled and annotated sequences for the genomes of the *T. gondii* reference strains have been deposited in GenBank at NCBI under accession codes GT1 (GCA_000149715.2), VEG (GCA_000150015.2), ME49 (GCA_000006565.2), MAS (GCA_000224865.2), RUB (GCA_000224805.2), CAST (GCA_000256705.1), TgCtBr5 (GCA_000259835.1), P89 (GCA_000224885.2), VAND (GCA_000224845.2), COUG (GCA_000338675.1), ARI (GCA_000250965.1), TgCtPRC2 (GCA_000256725.1), GAB2-2007-GAL-DOM2 (GCA_000325525.2), TgCtCo5 (GCA_000278365.1), FOU (GCA_000224905.2) and TgCtBr9 (GCA_000224825.1). Assembled and annotated sequences for the genomes of the *H. hammondi* reference strains have been deposited in GenBank at NCBI under accession code GCA_000258005.2. The annotation of reference genomes are also available at ToxoDB (<http://toxodb.org/common/downloads/White-PaperProvisionalGenomes/>): RNA-Seq reads for *T. gondii* strains have been deposited in the Sequence Read Archive at NCBI under accession codes GT1 (SRX099798) and ME49 (SRX099799). Sequence reads from the remaining *T. gondii* strains have been deposited in the Sequence Read Archive at NCBI under the following accession codes RH-88 (SRX160127, SRX160126), RH-JSR (SRX159850, SRX159851), TgCkCr1 (SRX160807), SOU (SRX160119), TgCkGy2 (SRX099785), CASTELLS (SRX099789), TgCatBr1 (SRX099790), TgCatBr18 (SRX099794), TgCatBr34 (SRX160051), BRC TgH 18002 GUY-KOE (SRX099796), BRC TgH 18003 GUY-MAT (SRX099783), GUY-2003-MEL

(SRX160131), GUY-2004-ABE (SRX160132), TgRsCr1 (SRX160143), TgCkBr141 (SRX160124), TgCatBr25 (SRX160134), TgCatBr10 (SRX099791), TgCatBr64 (SRX160743), BRC TgH 18001 GUY-DOS (SRX099782), TgCkCr10 (SRX099784), B41 (SRX099774), RAY (SRX099793), TgCatBr44 (SRX160141), GAB1-2007-GAL-DOM10 (SRX159841, SRX159839), GAB3-2007-GAL-DOM9 (SRX160125), GAB5-2007-GAL-DOM6 (SRX159842, SRX159840), TgCatPRC3 (SRX099799), BRC TgH 18009 (SRX157465), BRC TgH 18021 (SRX160041), BRC TgH 20005 (SRX157499, SRX171132), BRC TgH 21016 (SRX099775), GUY-2004-JAG1 (SRX099776), B73 (SRX159844, SRX159843), PRU (SRX099792), M7741 (SRX159890, SRX159849), ROD (SRX160129, SRX160128), TgShUS28 (SRX160130), BOF (SRX099774), GAB5-2007-GAL-DOM1 (SRX160069), TgCatBr26 (SRX099780), TgCatBr72 (SRX160049), TgDogCo17 (SRX099787), TgCatBr15 (SRX099779), G662M (SRX160052), GAB3-2007-GAL-DOM2 (SRX160123), TgCatBr3 (SRX160142) and TgH26044 (SRX160050).

Supplementary Information accompanies this paper at <http://www.nature.com/naturecommunications>

Competing financial interests: The authors declare no competing financial interests.

Reprints and permission information is available online at <http://npublishing.nature.com/reprintsandpermissions/>

How to cite this article: Lorenzi, H. *et al.* Local admixture of amplified and diversified secreted pathogenesis determinants shapes mosaic *Toxoplasma gondii* genomes. *Nat. Commun.* 7:10147 doi: 10.1038/ncomms10147 (2016).



This work is licensed under a Creative Commons Attribution 4.0 International License. The images or other third party material in this article are included in the article's Creative Commons license, unless indicated otherwise in the credit line; if the material is not included under the Creative Commons license, users will need to obtain permission from the license holder to reproduce the material. To view a copy of this license, visit <http://creativecommons.org/licenses/by/4.0/>